Preprint submitted to EarthArXiv

Incommensurate Global Cold-Seep Area Constructions and Their Consequences for an Iron-Bound Organic-Carbon Stock

Author

Luigi Caputi

Università Telematica San Raffaele, Via di Val Cannuta 247, 00166 Rome, Italy

Email: luigi.caputi1@gmail.com

Corresponding author

Peer-review status

Manuscript version: September 2, 2026

Incommensurate Global Cold-Seep Area Constructions and Their Consequences for an Iron-Bound Organic-Carbon Stock

Luigi Caputi[1,*]

[1]Università Telematica San Raffaele, Via di Val Cannuta 247, 00166 Rome, Italy

[*]Correspondence: luigi.caputi1@gmail.com

Version: September 2, 2026

Abstract

Global biogeochemical inventories require a spatial domain that is commensurate with the measured concentration, sediment mass, and ecosystem state. We re-evaluate the area term used by Ye et al. (2026) to estimate 142–218 Tg C of iron-bound organic carbon (Fe-OC) in the upper 30 cm of mature cold-seep sediment. Two primary results emerge. First, Ye et al. state that cold seeps occupy less than 0.05% of continental-slope area, citing a source that gives approximately 41 million km^2 of slope. That statement implies less than 2.05×10^4 km^2, yet the same article later applies $2.05–3.15 \times 10^5$ km^2 without a domain conversion. Second, the two values in that reported span are not shown to be bounds from a common estimator. The identifiable lower-source premises form a top-down slope-area–occupation calculation; the upper numerical fingerprint is a bottom-up extrapolation of an approximately 350-km^2 Haima field descriptor across a discovery-limited count of more than 900 seeps. The methods, spatial objects, sampling frames, and error structures are incommensurate, and "more than 900" cannot generate an upper bound at a nominal count of 900. Independent fluid-expulsion compilations and regional acoustic surveys document substantial inventory incompleteness and heterogeneity but do not supply a global active-sediment area. The absolute stock also contains an undisclosed sediment-mass coefficient: reproducing both endpoints with the reported depth and Fe-OC content requires an effective value near 1.65 g cm^{-3}. Interpreted as dry bulk density, this value is high relative to available regional and near-surface seep analogs, although not physically impossible. Replacing only 205,000 by the printed-premise product of 20,500 km^2 still changes the corresponding endpoint from about 142 to 14.2 Tg C, but this is a controlled sensitivity, not a new lower bound. The disclosed record therefore does not support interpreting the published area pair or derived stock span as empirical global intervals.

Keywords. cold seeps; iron-bound organic carbon; global area; spatial upscaling; dry bulk density; ecological succession.

1 Introduction

Global stock estimates commonly multiply a locally measured concentration by a sediment mass and a mapped or inferred spatial domain. The calculation is meaningful only when the area, material property, and ecosystem state refer to the same spatial object and target population. Cold seeps make this requirement unusually demanding: seepage is patchy and temporally variable, regional surveys detect different physical or biological indicators, and published inventories mix points, plumes, fields, carbonate structures, and active sediment patches [1, 10].

Ye et al. measured Fe-OC across developmental stages of marine cold seeps and extrapolated an average mature-seep value through the upper 0–30 cm of a reported global seep area of 2.05–3.15×10^5 km^2 [18]. They obtained 142–218 Tg C and framed the calculation as a possible long-term mature-seep reservoir, assuming that early-stage seeps eventually evolve toward mature seeps. The area was cited to Jiang et al. and Li et al. [7, 8].

The numerical area warrants analysis for reasons broader than an exponent. Ye et al.'s Introduction also states that cold seeps cover less than 0.05% of continental-slope area, citing Boetius and Wenzhöfer [18, 1]. Boetius and Wenzhöfer give approximately 41 million km^2 of continental slope and assume approximately 0.05% occupation by active seep systems. Those premises imply approximately 2.05×10^4 km^2, one-tenth of the later lower value. Moreover, Jiang et al.'s two reported endpoints trace numerically to heterogeneous constructions, while no common interval-generating method is disclosed.

We therefore ask four linked questions. Are the two area statements within Ye et al. mutually commensurate? Do the published endpoints define a scientific interval for a common global estimand? Does independent mapping support the scale or interpretation of either endpoint? And, once the spatial issue is separated from sediment mass and developmental stage, what can the published Fe-OC stock calculation defensibly represent? The objective is not to replace the reported span with another unsupported range. It is to identify which conclusions follow directly from the sources, which are supported interpretations, which calculations are conditional, and which global quantities remain unresolved.

2 Materials and methods

2.1 Source set and analytical distinctions

We used the versions of record and public supporting data for Boetius and Wenzhöfer, Jiang et al., Li et al., and Ye et al., together with primary literature on global slope masks, seep inventories, regional mapping, sediment physical properties, and seep succession [1, 7, 8, 18]. Sources and linked public records were checked through September 2, 2026.

Four evidentiary categories were kept separate. A *demonstrated result* follows from values or statements printed in the source record. A *supported interpretation* combines those observations with an explicit scientific model or comparison. A *conditional calculation* evaluates stated inputs while holding unmeasured terms fixed. An *unresolved quantity* lacks the observations needed for estimation. This terminology is used to prevent a numerical reconstruction from being mistaken for a measurement of true global seep area or stock.

2.2 Area reconstruction and commensurability tests

For the top-down construction, the printed occupation percentage converts to

$$0.05\% = 5 \times 10^{-4}, \tag{1}$$

and the nominal area is

$$A_{\text{slope}} = 41{,}000{,}000 \text{ km}^2 \times 5 \times 10^{-4} = 20{,}500 \text{ km}^2 = 2.05 \times 10^4 \text{ km}^2. \tag{2}$$

Holding the 41-million-km^2 domain fixed, 205,000 km^2 requires 0.5% occupation. Holding 0.05% fixed requires 410 million km^2 of slope. These inverse calculations test the scale of the disagreement without assuming how it arose.

For the upper numerical fingerprint, Li et al. state that the Haima active seep area is approximately 350 km^2, that more than 900 cold seeps had been found globally, and that other seeps were assumed to have areas comparable to Haima [8]. Evaluated at the nominal count 900,

$$A_{\text{Haima}} = 350 \text{ km}^2 \times 900 = 315{,}000 \text{ km}^2 = 3.15 \times 10^5 \text{ km}^2. \tag{3}$$

Because the count is explicitly greater than 900, Equation (3) is a numerical fingerprint rather than an upper bound.

We assessed whether the two constructions shared: (i) an estimand; (ii) a spatial unit; (iii) an activity and developmental-stage definition; (iv) a sampling frame and completeness model; and (v) an uncertainty-generating procedure. A pair was not treated as an interval merely because its values could be ordered.

2.3 Independent area context

Independent context was drawn from three bodies of published evidence. First, a global geomorphic map assigns 19,606,260 km^2 to continental slope, compared with the broader approximately 40–41-million-km^2 depth-defined margin or slope domain in the source chain [4, 9, 1]. Applying the same 0.05% assumption to the geomorphic mask gives 9,803 km^2. This is a denominator-definition sensitivity, not a confidence interval for seep area.

Second, we compared global and regional occurrence inventories. The SEAFLEA compilation contains more than 10,000 fluid-expulsion anomalies but is not a census of cold seeps: it is presence-only, incomplete, geographically biased, and deliberately combines current and recent-past indicators of several types [10]. Regional acoustic surveys report plumes or flares rather than active-sediment polygons. Skarke et al. detected approximately 570 plumes in 94,000 km^2 of the northern U.S. Atlantic margin and, using the upper-slope subset under stated geological and thermal conditions, conditionally suggested that tens of thousands of seeps could be discoverable on passive margins [13]. Serov et al. mapped 21,703 flares in a 4,892-km^2 Barents Sea hydrocarbon-leakage region [12]. We used these observations to test transferability of a global count or density, not to estimate area.

Third, we examined the spatial object represented by Haima. Yao et al. repeat a literature descriptor of a 618-km^2 field containing a 350-km^2 area reported as active; they did not derive that polygon [17]. Xu et al. framed the field-wide scale of seepage activity as poorly known; their 17 high-resolution dives observed at least six individual community and/or carbonate-mound patches [16]. These scales are not interchangeable with a globally enumerated point called a "seep."

We also considered whether global methane budgets could independently constrain area. Ocean-to-atmosphere methane transfer depends strongly on release depth, bubble properties, dissolution, and oxidation; deep-seep methane commonly fails to reach the atmosphere [15]. Without a representative distribution of footprint-specific seabed flux and water-column transfer, an atmospheric or oceanic methane budget cannot be inverted to active-sediment area.

2.4 Fe-OC concentration, sediment mass, and stock sensitivity

Ye et al. report mature-seep Fe-OC content of $0.14 \pm 0.06\%$ of sediment dry mass [18]. We recalculated arithmetic means and sample standard deviations from the public source rows. The current-study mature block contains 14 depth-interval rows; the historical mature block contains eight rows from Hu et al. [5]. The pooled 22-row calculation was used only to reproduce the printed summary. Because the rows are depth intervals rather than 22 independent sites, we also compared the two source-block means with equal weight and did not interpret either calculation as a globally representative estimator.

For area A in km^2, depth z in m, dry bulk density ρ_d in g cm^{-3}, and Fe-OC content c in percent of sediment dry mass, dimensional mass balance gives

$$M_{\mathrm{Tg}} = Az\rho_d \frac{c}{100}. \tag{4}$$

The powers of ten from km^2 to m^2, g cm^{-3} to g m^{-3}, and g to Tg cancel in this compact expression. Since c is defined per unit dry sediment mass, the commensurate physical coefficient is dry solid mass per unit bulk volume, not saturated bulk density.

Ye et al. disclose A, $z = 0.30$ m, and $c = 0.14\%$, but the article, supporting information, and public source files do not state the stock equation or the coefficient used to convert sediment volume into dry sediment mass. Reverse-engineering the rounded endpoints yields an endpoint-compatible effective coefficient near 1.65 g cm^{-3}. This is an algebraic reconstruction only: it does not establish the coefficient's physical definition, provenance, or exact unrounded value, and it does not show that Ye et al. selected 1.65 as either dry or saturated bulk density.

We evaluated conditional stocks at three coefficients: 0.9 g cm^{-3}, the mean dry bulk density measured in a Qiongdongnan core and applied by Chen et al. to a seep-influenced core approximately 35 km away; 1.3 g cm^{-3}, the dry-density assumption used in the Jiang and Li studies; and the endpoint-compatible 1.65 g cm^{-3} [3, 7, 8]. These comparators are not a probability distribution and are not measurements of Ye et al.'s 0–30-cm samples.

As a physical diagnostic, the two-phase relation

$$\rho_d = \rho_g(1 - \phi) \tag{5}$$

links dry bulk density to grain density ρ_g and porosity ϕ. Riedel et al. measured a mean grain density near 2.70 g cm^{-3} at a hydrate-margin analog [11]. As a conditional diagnostic, if the endpoint-compatible effective coefficient were interpreted as dry bulk density, setting $\rho_d = 1.65$ g cm^{-3} would imply $\phi = 0.389$. We compared that diagnostic with regional and hydrate-margin literature while retaining lithology, cementation, shell content, and burial depth as limitations [14, 6].

Finally, the lower-area substitution was evaluated without selecting a density:

$$M_{\mathrm{conditional}} = 142 \text{ Tg C} \times \frac{20{,}500}{205{,}000} = 14.2 \text{ Tg C}. \tag{6}$$

If both published whole-Tg endpoints were produced by one area-linear coefficient and rounded conventionally, their joint coefficient interval gives a corrected lower result of $[14.1548, 14.2198)$ Tg C. Thus the approximate 14.2 value is robust to endpoint rounding but remains conditional on the published non-area terms.

2.5 Developmental-stage domain

Let A_a denote the current area of all active seeps, A_m the current area of active mature seeps, and $f_m = A_m/A_a$. If the footprint classified as currently active and mature is nested within a consistently delineated current-active footprint, a current mature-only stock is

$$M_m = c_m A_m K = c_m f_m A_a K, \tag{7}$$

where K contains depth and sediment mass per unit area. Holding c_m and K fixed, substituting A_a for A_m multiplies the mature-only result by $1/f_m$; this is upward if $0 < f_m < 1$ and unchanged if $f_m = 1$. For an area-only comparison of stock across all active stages that also holds K fixed across stages,

$$M_a = \bar{c}_a A_a K, \qquad \widehat{M}_a = c_m A_a K, \tag{8}$$

so the sign of the difference depends on $c_m - \bar{c}_a$. Without a common K, it also depends on stage-specific sediment mass per unit area. Ye et al.'s stated eventual-mature scenario is a third estimand and requires the additional, untested equality $A_{\text{future},m} = A_{\text{current},a}$. These three targets were evaluated separately.

3 Results

3.1 Ye et al. contain an unresolved area-scale inconsistency

Ye et al.'s statement that cold seeps occupy less than 0.05% of continental-slope area corresponds to less than 20,500 km^2 when paired with the 41-million-km^2 domain in the cited source. Section 4.3 nevertheless applies 205,000–315,000 km^2. Expressed on the same 41-million-km^2 domain, those values equal 0.500% and 0.768%, respectively: 10.0 and 15.4 times the 0.05% premise. Under Ye et al.'s strict "less than" wording, the lower disagreement is greater than tenfold.

No spatial-domain or seep-category conversion is supplied between the two statements. The comparison does not establish that Ye et al. calculated 205,000 km^2 directly from the 0.05% premise; they cite Jiang et al. and Li et al. for the later value. It demonstrates an unreconciled within-article scale and domain inconsistency. A materially broader object could in principle occupy a larger area, but that object and its conversion would need to be defined.

3.2 The reported span is not shown to derive from a common interval-generating method

Jiang et al. print 2.05–3.15×10^5 km^2 while jointly citing Boetius and Wenzhöfer and Li et al., without endpoint-specific derivations [7]. The lower mantissa matches Equation (2) while its exponent is one power of ten larger. Equation (3) matches the upper value at a nominal count of 900. This source association is a strong numerical-provenance interpretation rather than explicit endpoint citation syntax. No common interval-generating method is disclosed in Jiang et al. or in the cited source passages.

The two constructions differ in spatial object, sampling frame, inventory completeness, clustering, overlap, and uncertainty structure, and are not shown to share an activity definition or representative target population (Table 1). Consequently, changing the lower exponent alone

Table 1. The two identifiable constructions associated with the reported global cold-seep area span.

Feature	Slope-occupation construction	Haima-count construction	Consequence
Method	Continental-slope domain multiplied by assumed active-seep occupation	One field-scale area multiplied by a global discovery count	Top-down and bottom-up scalings are not shown to share an estimator
Nominal inputs	41 million km^2 and approximately 0.05%	Approximately 350 km^2 and more than 900 seeps	Inputs represent different spatial objects, units of analysis, and sampling frames
Nominal output	2.05×10^4 km^2	3.15×10^5 km^2 at exactly 900	The printed 2.05×10^5 lower value is not generated by the first premises
Bound status	Assumed occupation scenario; not a lower confidence limit	At exactly 900 the nominal product is 3.15×10^5 km^2; a count stated as greater than 900 cannot make that value an upper limit	The ordered pair has no disclosed statistical coverage interpretation

would not show that the resulting 2.05×10^4–3.15×10^5 km^2 pair is a valid interval. It would pair a corrected nominal product with an incommensurate extrapolation.

3.3 Independent evidence does not calibrate a global active-seep area

The slope denominator itself is definition-sensitive. Applying 0.05% to the 19.606-million-km^2 geomorphic slope mask gives approximately 9,803 km^2, whereas applying it to 41 million km^2 gives 20,500 km^2. Both remain on the order of 10^4 km^2. Conversely, 205,000–315,000 km^2 require 0.50–0.77% occupation of the 41-million-km^2 domain or 1.05–1.61% of the geomorphic slope mask. Those are materially different occupation hypotheses, not uncertainty generated by the printed 0.05% assumption.

The independent literature therefore supports two qualitative conclusions: fluid-expulsion occurrence compilations are incomplete, and observed densities and spatial objects are highly heterogeneous (Table 2). It does not select 20,500, 205,000, or 315,000 km^2 as a measured global area. In particular, a growing discovery count cannot be converted to area without a defined footprint distribution, sampling design, treatment of overlapping features, and activity time window.

3.4 The concentration is reproducible, but the sediment-mass coefficient is not disclosed

The 14 current-study mature depth rows have mean 0.108571% and sample SD 0.024133%; the eight Hu et al. mature rows have mean 0.195000% and sample SD 0.055806%. Pooling all 22 rows yields $0.140000 \pm 0.056653\%$, which rounds to Ye et al.'s $0.14 \pm 0.06\%$. Equal

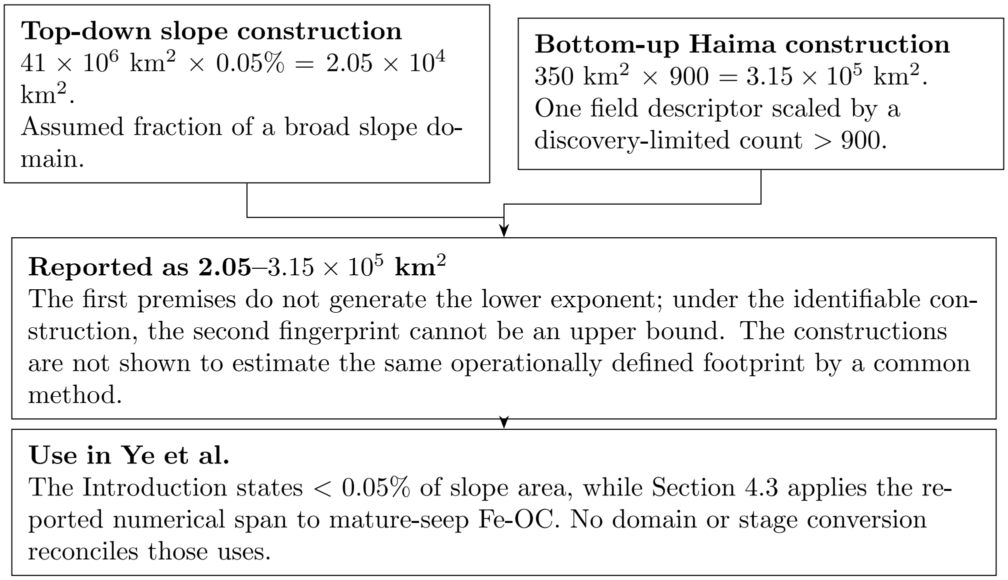

Figure 1. Two heterogeneous area constructions and their downstream use. The arrows show the numerical and citation relationships evaluated here; source association is based on joint citation and numerical fingerprints. The central scientific problem is lack of a disclosed common operational estimand and interval-generating method.

weighting of the two source-block means gives 0.151786%. The numerical match shows that the printed concentration can be reproduced by row pooling, but the public files do not specify that aggregation rule and the rows are not independent global sampling units.

The current-study early-stage rows have mean 0.164286±0.041542%, compared with 0.108571± 0.024133% for the current-study mature rows. These local data do not estimate global stage means, but they show that a higher mature-stage concentration cannot be assumed when determining the sign of a stage-substitution bias.

With A, z, and c fixed at the published values, an effective coefficient near 1.65 g cm^{-3} reproduces both whole-Tg stock endpoints. Interpreted as dry bulk density, it implies porosity 0.389 at the 2.70-g-cm^{-3} mean grain density measured by Riedel et al. That is lower than the approximately 0.55–0.75 near-surface porosities reported from the same hydrate-margin study, and lower than the 0.65 porosity assumed in Haima flux calculations [11, 14]. Chen et al.'s regional mean dry bulk density of 0.9 g cm^{-3} was measured outside the seep and averaged over a longer core before being applied to a seep-influenced core 35 km away; it is context rather than a replacement measurement [3]. Conversely, a Haima hydrate-reservoir study reports a calculated porosity of 0.40 without sampling depth or raw physical-property values, providing a regional counterexample to treating 0.40 as impossible while not establishing that value for the upper 30 cm [6].

Table 3 is a sensitivity analysis, not a set of confidence limits. No cited value is a globally representative measurement for the upper 30 cm of mature seep sediment. The defensible result is that the physical basis of the absolute mass conversion is undisclosed and consequential; neither endpoint agreement nor the physical diagnostics identifies the coefficient as dry or saturated bulk density, and a specific density error is not demonstrated.

Table 2. Independent observations constrain occurrence and heterogeneity but not global active-sediment area.

Observation	Spatial object	Relevance to global area
Global SEAFLEA compilation: $> 10{,}000$ anomalies, not a cold-seep count [10]	Presence-only mixture of plumes, pockmarks, hardgrounds, communities, and other current or recent-past indicators	Demonstrates inventory incompleteness and object mixing; encounter probability is not fractional active-sediment cover
Northern U.S. Atlantic: ~ 570 plumes in 94,000 km^2 [13]	Acoustic water-column plumes in a systematic regional survey	Supports many undiscovered occurrences; does not measure the footprint of sediment influenced by each plume
Northern Norwegian Barents Sea: 21,703 flares in 4,892 km^2 [12]	Acoustic flares in a hydrocarbon-leakage region containing an intense hotspot	Raw density is over 700 times the U.S. Atlantic value; geology, survey design, and definitions prevent global transfer
Haima field: literature-reported 350-km^2 active descriptor and at least six dive-observed community and/or carbonate-mound patches [17, 16]	Field-scale descriptor versus discrete biological and carbonate observations	Shows why multiplying one field descriptor by a point count mixes units of analysis

3.5 The developmental-stage effect depends on the target quantity

Ye et al.'s mature sampling sites were actively seeping, and the succession framework they cite describes mature, mussel-bearing communities as persisting while methane flux continues [18, 2]. This nesting is a conditional, set-theoretic relation within a consistently delineated current-active footprint; it does not show that independently published "mature" and "active" areas use the same activity criterion or spatial boundary. Under that condition, if the target is a current mature-only stock, substituting total active area for mature area multiplies the result by $1/f_m$ while c_m and K are held fixed. The substitution is upward if $0 < f_m < 1$ and unchanged if $f_m = 1$; the global mature fraction f_m is unknown.

That directional result does not extend to two other targets. For a current stock across all active stages, the sign depends on the area-weighted stage concentrations only if depth and sediment mass per unit area are held fixed; otherwise it also depends on stage-specific sediment-mass coefficients. Ye et al.'s current-study early-stage mean exceeds its mature-stage mean. For Ye et al.'s stated eventual-mature scenario, using present active area requires the untested assumption that the active footprint is conserved as systems mature. Expansion, contraction, cessation, displacement, and unequal stage duration leave the direction unresolved. A stage-commensurate spatial basis is therefore not established; the bias is conditional on the target estimand and is not unconditionally upward.

Table 3. Conditional Fe-OC stock sensitivity to the sediment-mass coefficient. All rows hold depth at 0.30 m and Fe-OC content at 0.14%.

Coefficient context	ρ_{eff} (g cm^{-3})	20,500 km^2 (Tg C)	205,000 km^2 (Tg C)	315,000 km^2 (Tg C)
Regional dry-density comparator [3]	0.9	7.75	77.49	119.07
Dry-density assumption used by Jiang and Li [7, 8]	1.3	11.19	111.93	171.99
Endpoint-compatible effective value	1.65	14.21	142.07	218.30

4 Discussion

4.1 The central result is not an arithmetic replacement

Equation (2) establishes that the printed 41-million-km^2 and 0.05% premises yield 2.05×10^4 km^2. The same order-of-magnitude conflict is visible within Ye et al. itself, independently of any reconstruction of how Jiang et al.'s exponent arose. This makes the inconsistency a scientific result about the stated spatial domain, not merely a comment on citation history.

More importantly, the reported endpoints are not shown by the disclosed record to define a valid global interval. The lower-source construction is a fraction of a broad slope domain. The upper numerical fingerprint treats one field-scale descriptor as representative of every discovered seep. Correcting one exponent while retaining the other endpoint would preserve the deeper problem. Neither 2.05–3.15×10^5 km^2 nor 2.05×10^4–3.15×10^5 km^2 is supported by the disclosed record as lower and upper bounds on simultaneously active cold-seep sediment.

Independent observations strengthen this conclusion rather than resolving it. They show many unrecorded or variably detected seep indicators, enormous regional heterogeneity, and non-equivalence among points, plumes, fields, and habitat patches. They do not provide a representative distribution of active-sediment footprints from which global coverage can be estimated. The current evidence supports an order-of-magnitude conditional statement: the printed 0.05% assumption produces an area on the order of 10^4 km^2 under two published denominator or domain definitions, whereas areas on the order of 10^5 km^2 require a materially different occupation hypothesis. It does not establish that either scale is the true global area.

4.2 Consequences for the Fe-OC stock

The 14.2-Tg result remains useful, but only for a precise purpose. It shows the consequence of changing one area input by a factor of ten while preserving the published area-linear mapping. It is not a corrected global lower bound because 20,500 km^2 is itself the output of an assumed occupation fraction and because the 315,000-km^2 value is not supported as a commensurate upper limit. The density-independent rounding analysis confirms the arithmetic consequence; it does not validate the underlying area.

The dry-density analysis adds a separate limitation to absolute stock magnitude. Because Fe-OC is expressed per dry sediment mass, the stock calculation requires a coefficient that converts bulk sediment volume into dry sediment mass; in Equation (4), that coefficient is dry bulk density. The need to define it can be illustrated without attributing a method to Ye et al.: at porosity 0.65, grain density 2.70 g cm^{-3}, and porewater density 1.024 g cm^{-3}, the two-phase relations give a dry bulk density of 0.945 g cm^{-3} and a saturated bulk density of 1.61 g cm^{-3}. These are different physical quantities, and substituting saturated density for dry bulk density would include porewater mass in an inventory defined per unit dry sediment mass. Although 1.61 is numerically near the endpoint-compatible effective coefficient of 1.65 g cm^{-3}, proximity alone does not identify the coefficient's provenance or physical meaning and is not evidence that Ye et al. used saturated density. Cementation, shell content, grain-size distribution, compaction, rounding, or other undisclosed mass terms could also affect the effective value. This dimensional diagnostic demonstrates why the stock equation and the coefficient's definition, value, source, and aggregation must be disclosed; it supports an unresolved mass-conversion method, not a wet-versus-dry attribution.

The stage analysis similarly changes interpretation rather than producing a correction factor. A current mature-only inventory requires the global mature fraction of active area. An all-active inventory requires stage-specific stock per unit area, including concentration and sediment-mass coefficients. A future mature scenario requires a dynamic model of footprint persistence and stage duration. None of those quantities is supplied by a stage-unspecific global area.

4.3 Requirements for a defensible global estimate

A defensible global seep-area estimate would first define the mapping unit: active sediment patch, biological community, acoustic vent, carbonate field, or broader geologic system. It would define an activity window and developmental stage; use a survey design that models detection and unsurveyed regions; estimate a distribution of footprint sizes rather than applying one exemplar; and treat overlap and clustering explicitly. A stock estimate would then pair that area with stage-matched Fe-OC concentrations, sample-matched dry bulk density, layer thickness, and a transparent aggregation model.

These requirements do not weaken Ye et al.'s sediment observations. The public rows reproduce their central concentration summary, and the developmental comparison remains scientifically informative. The unresolved step is the transition from local, depth-resolved observations to a global spatial inventory. Until a common estimand and sampling model are disclosed and supported, global Fe-OC storage should be reported as scenario-dependent sensitivity rather than as a bounded stock.

5 Limitations

This study does not produce new global seep mapping and cannot estimate true active-seep area. Jiang et al. do not assign individual citations to individual endpoints, so the endpoint-source mapping rests on distinctive numerical fingerprints and citation context, although the lack of a disclosed common interval method is independent of that mapping. Regional occurrence surveys use different instruments, thresholds, clustering rules, and geological settings; their raw densities demonstrate heterogeneity but are not mutually calibrated.

The density comparators are not measurements of Ye et al.'s sampled upper 30 cm. Porosity and dry bulk density vary with lithology, carbonate cementation, shells, organic matter, coring disturbance, salt correction, and depth, and neither the analog comparison nor the wet-versus-dry diagnostic identifies the coefficient used by Ye et al. The pooled Fe-OC reconstruction weights depth rows, and the public data do not define globally representative sites or a published aggregation rule. Finally, no global stage-resolved area data establish f_m or future footprint persistence. These limitations leave the absolute global area and stock unresolved while preserving the demonstrated arithmetic and the supported commensurability and reporting conclusions.

As normal scientific due diligence before submission, the corresponding authors of Jiang et al. should be invited to clarify the derivation, operational area definition, endpoint attribution, and intended interval interpretation of the reported area span; the corresponding authors of Ye et al. should be invited to clarify their use of that area and the stock equation and sediment-mass coefficient used to obtain 142–218 Tg C. Any documented clarification received before submission should be incorporated or reported transparently; the present analysis relies only on the published record.

6 Conclusion

The strongest findings are two linked spatial-upscaling problems. Ye et al. contain an unreconciled order-of-magnitude inconsistency between a stated $< 0.05\%$ occupation of continental-slope area and the 2.05–3.15×10^5 km^2 area later applied. The identifiable source premises numerically associate that span with a slope-occupation calculation and a single-field–times–site-count extrapolation; the disclosed record does not show that its endpoints are lower and upper bounds from a common estimator.

Independent compilations and regional surveys indicate that seep indicators are widespread, incompletely observed, and highly heterogeneous, but they do not validate a global active-sediment area. The Fe-OC concentration can be reproduced from public rows, whereas the sediment-mass coefficient needed for the absolute stock is undisclosed. The endpoint-compatible effective value would be high relative to available shallow-sediment context if interpreted as dry bulk density, but the published record does not identify it as dry or saturated bulk density. Developmental stage introduces a further target-domain requirement: under a nested current mature-only model, area substitution cannot bias the result downward and is upward only when $f_m < 1$; for all-active or eventual-mature targets, its direction remains unresolved.

Replacing 205,000 by the nominal 20,500-km^2 product changes the corresponding 142-Tg endpoint to approximately 14.2 Tg C. That result is a robust conditional sensitivity, not a new global lower bound. The published record does not support interval interpretation of the area pair; the resulting global Fe-OC stock remains unresolved until area, stage, and sediment mass are estimated on commensurate bases.

7 Data and code availability

The numerical reconstructions, source-derived tables, source-value record, and executable tests are distributed with this manuscript and in the accompanying repository. The retained scripts reproduce the area arithmetic, Fe-OC row summaries, denominator sensitivity, density sensitivity, endpoint-rounding bounds, and stage-domain formulas using only the Python standard library. Third-party publications are linked by DOI rather than redistributed.

AI and Programmatic Research Provenance Statement

The originating hypothesis, initial formulation, and initial structure of this work were generated and provided by UCP Technology LLC through its programmatic research process. The source record for the originating research candidate and subsequent development is maintained at: https://github.com/joe-ucp/Luigi2

Artificial intelligence was used as a computational component of that process to generate and develop the originating research candidate, including the initial theoretical formulation, research development, manuscript drafting, literature-supported development, and computational verification. Artificial intelligence was not used to provide the independent scientific judgment determining whether the work was correct, useful, novel, or suitable for publication.

The human author independently evaluated, revised, verified, interpreted, and approved the final work.

References

[1] A. Boetius and F. Wenzhöfer, Seafloor oxygen consumption fuelled by methane from cold seeps, *Nature Geoscience* **6** (2013), 725–734. https://doi.org/10.1038/ngeo1926.

[2] D. A. Bowden, A. A. Rowden, A. R. Thurber, A. R. Baco, L. A. Levin, and C. R. Smith, Cold seep epifaunal communities on the Hikurangi Margin, New Zealand: Composition, succession, and vulnerability to human activities, *PLOS ONE* **8** (2013), e76869. https://doi.org/10.1371/journal.pone.0076869.

[3] Y. Chen, L. Dong, W. Sui, M. Niu, X. Cui, K.-U. Hinrichs, and F. Wang, Cycling and persistence of iron-bound organic carbon in subseafloor sediments, *Nature Communications* **15** (2024), Article 6370. https://doi.org/10.1038/s41467-024-50578-5.

[4] P. T. Harris, M. Macmillan-Lawler, J. Rupp, and E. K. Baker, Geomorphology of the oceans, *Marine Geology* **352** (2014), 4–24. https://doi.org/10.1016/j.margeo.2014.01.011.

[5] Y. Hu, K. Li, J. C. Faust, J. Peckmann, D. Zhang, L. Chen, Q. Liang, D. Chen, and D. Feng, Stability of reactive iron-bound organic carbon during sulfidization of iron oxides: Insights from methane-seep sediments, *Geophysical Research Letters* **52** (2025), e2024GL112119. https://doi.org/10.1029/2024GL112119.

[6] Y. Huang, J.-C. Feng, Y. Xie, Y. Wang, P. Li, and M. Zhang, Phase equilibrium characteristics of natural gas hydrate formation at the deep-water environment of "Haima" cold seep, *Energy Reports* **8** (2022), 5501–5509. https://doi.org/10.1016/j.egyr.2022.04.011.

[7] Q. Jiang, L. Cao, Y. Han, et al., Cold seeps are potential hotspots of deep-sea nitrogen loss driven by microorganisms across 21 phyla, *Nature Communications* **16** (2025), Article 1646. https://doi.org/10.1038/s41467-025-56774-1.

[8] J. Li, X. Dong, Y. Tang, et al., Deep sea cold seeps are a sink for mercury and source for methylmercury, *Communications Earth & Environment* **5** (2024), Article 324. https://doi.org/10.1038/s43247-024-01484-7.

[9] L. Menot, M. Sibuet, R. S. Carney, et al., New perceptions of continental margin biodiversity, in A. D. McIntyre (ed.), *Life in the World's Oceans: Diversity, Distribution and Abundance*, Wiley-Blackwell, 2010, pp. 79–102. https://doi.org/10.1002/9781444325508.ch5.

[10] B. J. Phrampus, T. R. Lee, and W. T. Wood, A global probabilistic prediction of cold seeps and associated SEAfloor FLuid Expulsion Anomalies (SEAFLEAs), *Geochemistry, Geophysics, Geosystems* **21** (2020), e2019GC008747. https://doi.org/10.1029/2019GC008747.

[11] M. Riedel, P. Long, C.-S. Liu, P. Schultheiss, T. Collett, and the ODP Leg 204 Shipboard Scientific Party, Physical properties of near-surface sediments at southern Hydrate Ridge: Results from ODP Leg 204, *Proceedings of the Ocean Drilling Program, Scientific Results* **204** (2006), 1–29. https://doi.org/10.2973/odp.proc.sr.204.104.2006.

[12] P. Serov, K. Andreassen, M. Winsborrow, R. Mattingsdal, and H. Patton, Geological and glaciological controls of 21,700 active methane seeps in the northern Norwegian Barents Sea, *Frontiers in Earth Science* **12** (2024), 1404027. https://doi.org/10.3389/feart.2024.1404027.

[13] A. Skarke, C. Ruppel, M. Kodis, D. Brothers, and E. Lobecker, Widespread methane leakage from the sea floor on the northern U.S. Atlantic margin, *Nature Geoscience* **7** (2014), 657–661. https://doi.org/10.1038/ngeo2232.

[14] L. Tang, J.-C. Feng, C.-R. Li, X. Chen, H. Zhang, and S. Zhang, Distribution and potential drivers of methane emissions from deep-sea environments in Haima cold seep areas, *Frontiers in Marine Science* **12** (2025), 1714180. https://doi.org/10.3389/fmars.2025.1714180.

[15] T. Weber, N. A. Wiseman, and A. Kock, Global ocean methane emissions dominated by shallow coastal waters, *Nature Communications* **10** (2019), Article 4584. https://doi.org/10.1038/s41467-019-12541-7.

[16] H. Xu, M. Du, J. Li, et al., Spatial distribution of seepages and associated biological communities within Haima cold seep field, South China Sea, *Journal of Sea Research* **165** (2020), 101957. https://doi.org/10.1016/j.seares.2020.101957.

[17] G. Yao, H. Zhang, P. Xiong, H. Jia, Y. Shi, and M. He, Community characteristics and genetic diversity of macrobenthos in Haima cold seep, *Frontiers in Marine Science* **9** (2022), 920327. https://doi.org/10.3389/fmars.2022.920327.

[18] W. Ye, Y. Chen, C. Yang, et al., Dynamics of iron-bound organic carbon across different development stages of marine cold seeps, *Global Biogeochemical Cycles* **40** (2026), e2025GB008889. https://doi.org/10.1029/2025GB008889.